MRG15-mediated tethering of PALB2 to unperturbed chromatin protects active genes from genotoxic stress

Jean-Yves Bleuyard[a], Marjorie Fournier[a], Ryuichiro Nakato[b], Anthony M. Couturier[a], Yuki Katou[b], Christine Ralf[a], Svenja S. Hester[c], Daniel Dominguez[d], Daniela Rhodes[e], Timothy C. Humphrey[f], Katsuhiko Shirahige[b], and Fumiko Esashi[a,1]

[a]Sir William Dunn School of Pathology, University of Oxford, Oxford, OX1 3RE, United Kingdom; [b]Research Center for Epigenetic Disease, Graduate School of Frontier Sciences, The University of Tokyo, Tokyo 113-0032, Japan; [c]Advanced Proteomics Facility, Department of Biochemisty, University of Oxford, Oxford, OX1 3QU, United Kingdom; [d]Department of Biology, Massachusetts Institute of Technology, Cambridge, MA 02139-4307; [e]NTU Institute of Structural Biology, Nanyang Technological University, 636921 Singapore; and [f]Cancer Research UK/Medical Research Council Oxford Institute for Radiation Oncology, Department of Oncology, University of Oxford, Oxford, OX3 7DQ, United Kingdom

Edited by James E. Haber, Brandeis University, Waltham, MA, and approved May 16, 2017 (received for review December 9, 2016)

The partner and localiser of BRCA2 (PALB2) plays important roles in the maintenance of genome integrity and protection against cancer. Although PALB2 is commonly described as a repair factor recruited to sites of DNA breaks, recent studies provide evidence that PALB2 also associates with unperturbed chromatin. Here, we investigated the previously poorly described role of chromatin-associated PALB2 in undamaged cells. We found that PALB2 associates with active genes through its major binding partner, MRG15, which recognizes histone H3 trimethylated at lysine 36 (H3K36me3) by the SETD2 methyltransferase. Missense mutations that ablate PALB2 binding to MRG15 confer elevated sensitivity to the topoisomerase inhibitor camptothecin (CPT) and increased levels of aberrant metaphase chromosomes and DNA stress in gene bodies, which were suppressed by preventing DNA replication. Remarkably, the level of PALB2 at genic regions was frequently decreased, rather than increased, upon CPT treatment. We propose that the steady-state presence of PALB2 at active genes, mediated through the SETD2/H3K36me3/MRG15 axis, ensures an immediate response to DNA stress and therefore effective protection of these regions during DNA replication. This study provides a conceptual advance in demonstrating that the constitutive chromatin association of repair factors plays a key role in the maintenance of genome stability and furthers our understanding of why PALB2 defects lead to human genome instability syndromes.

PALB2 | MRG15 | SETD2 | DNA replication | transcription

Inherited mutations in the partner and localiser of BRCA2 (*PALB2*) gene predispose to breast and pancreatic cancer (1–3) and also congenital malformations, growth retardation, and early childhood cancer in a rare subgroup of Fanconi anemia (FA-N) patients (4, 5). The best characterized function of PALB2 is to physically link the two main breast cancer susceptibility gene products, BRCA1 and BRCA2, at sites of DNA damage (6–8), thus playing a pivotal role in the repair of DNA double-strand breaks (DSBs) by homologous recombination (HR). BRCA1 facilitates DNA-end resection to produce single-stranded (ss) DNA (9) and concomitantly attracts PALB2, together with BRCA2 and RAD51, to DSB sites (6–8). In turn, BRCA2 promotes the loading of the RAD51 recombinase onto ssDNA (10–12), which is critical for the strand invasion and exchange phase of HR (13). This mechanism of repair factor recruitment is important for the timely activation of HR at sites of DNA damage, and its perturbation in individuals with impaired PALB2 function is presumed to cause human pathologies.

Although PALB2 is commonly described as a repair factor recruited to sites of DNA breaks, we and others have provided evidence that PALB2 also associates with chromatin in the absence of DNA damage (14–17). A recent genome-wide analysis of PALB2 chromatin occupancy revealed enrichment at highly active genes, with PALB2 occupying the entire body of these genes (18). PALB2 was shown to support the transcription of a subset of NF-κB– and retinoic acid-responsive genes. However, PALB2 does not behave as a general transcription coactivator, and the physiological significance of its association with active genes remains unclear.

Here, we provide direct evidence that PALB2 associates with active genes through its major binding partner MRG15 (MORF-related gene on chromosome 15). Cells expressing a PALB2 variant, harboring missense mutations that hinder MRG15 binding, exhibit elevated sensitivity to the topoisomerase I (TOP1) inhibitor camptothecin (CPT) and increased levels of aberrant metaphase chromosomes and DNA stress in gene bodies, which were suppressed by preventing DNA replication. Collectively, our findings suggest that steady-state chromatin association of PALB2 contributes to protecting active genes from stress arising during DNA replication and give insights into the way in which PALB2 defects elicit human genome instability syndromes.

Results and Discussion

PALB2 Associates with Active Genes Through the SETD2/H3K36me3/MRG15 Axis. To gain insights into the mechanism of PALB2 association with undamaged chromatin, PALB2 binding partners in exponentially growing cells were identified by quantitative mass spectrometry (MS). This analysis revealed MRG15 and the product of another MORF-related gene on chromosome X (MRGX) as the two major binding partners of PALB2 (Fig. 1*A*

Significance

Partner and localiser of BRCA2 (PALB2) is a breast cancer susceptibility gene, and the role of its product in repairing broken chromosomes has been extensively described. However, a fraction of PALB2 is also found on intact chromosomes, and it is unknown how and why PALB2 associates with undamaged chromatin. In this study, we establish that the histone binding protein MRG15 is a major interaction partner of PALB2 and plays a key role in tethering PALB2 to active genes. Failure of PALB2 to interact with MRG15 leads to the accumulation of DNA stress at active genes and chromosome instability in dividing cells. These findings shed light on why patients with PALB2 mutations often develop genome instability syndromes, such as cancer.

Author contributions: J.-Y.B. and F.E. designed research; J.-Y.B., M.F., Y.K., C.R., and S.H. performed research; M.F., R.N., A.M.C., D.R., T.C.H., and K.S. contributed new reagents/analytic tools; J.-Y.B., M.F., R.N., A.M.C., D.D., and F.E. analyzed data; and J.-Y.B. and F.E. wrote the paper.

The authors declare no conflict of interest.

This article is a PNAS Direct Submission.

Freely available online through the PNAS open access option.

Data deposition: Proteomics and ChIP-sequencing datasets are available via ProteomeXchange (identifier PXD006391) and NCBI-SRA (accession no. SRP105310), respectively.

[1]To whom correspondence should be addressed. Email: fumiko.esashi@path.ox.ac.uk.

This article contains supporting information online at www.pnas.org/lookup/suppl/doi:10.1073/pnas.1620208114/-/DCSupplemental.

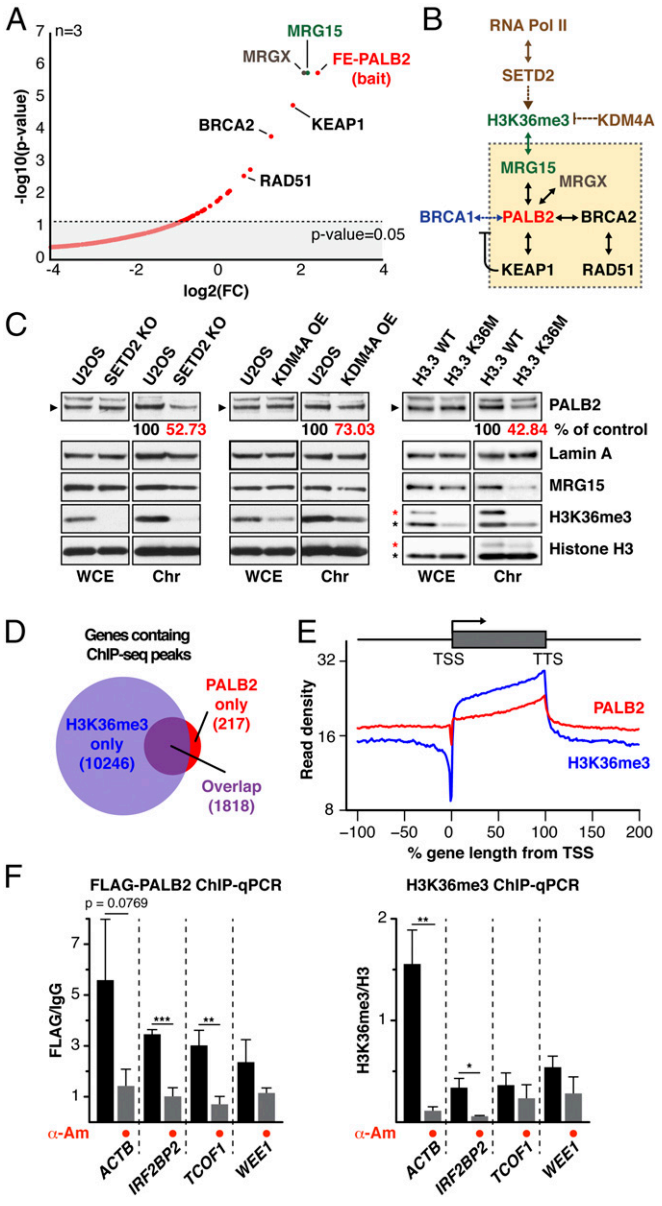

Fig. 1. MRG15, SETD2, and H3K36me3 are required for PALB2 chromatin association in unperturbed cells. (*A*) Volcano plot showing FLAG-EGFP-PALB2 (FE-PALB2)-associated proteins identified by MS. The log2 of the fold change (FC) over a FLAG-EGFP control was plotted against negative log10 *P* values ($n = 3$). (*B*) Schematic of the pathway linking transcription and PALB2. (*C*) WB analysis of PALB2 in the chromatin fraction of U2OS cells with CRISPR SETD2 knockout (*Left*), KDM4A overexpression (OE) (*Middle*), and wild type (WT) or mutant (K36M) histone variant H3.3 overexpression (*Right*). Asterisks indicate endogenous H3 (black) and exogenous H3.3 (red). (*D*) Venn diagram showing the overlap of H3K36me3-containing and PALB2-bound genes. (*E*) The averaged profile of H3K36me3 and PALB2 around gene loci with H3K36me3 peaks. Read density (*y* axis) is normalized for total number of mapped reads. (*F*) ChIP-qPCR quantification of FLAG-PALB2 (*Left*) and H3K36me3 (*Right*). Mean values ± SD ($n = 3$, with triplicate qPCR reactions). Where indicated, cells were treated with α-Am. Asterisks indicate two-tailed paired Student's *t* test; $*P < 0.05$, $**P < 0.01$, $***P < 0.001$.

and Dataset S1). Significantly, depletion of MRG15, but not MRGX or BRCA1, impaired PALB2 and BRCA2 chromatin association (Fig. S1 *A*–*C*; see also chromatin association of the PALB2 variant ablating BRCA1 binding in Fig. 2), suggesting a specific role for MRG15 in the recruitment of the PALB2–BRCA2 complex to unperturbed chromatin.

In addition to an MRG domain, which binds various transcriptional regulators and chromatin-remodeling factors, MRG15 contains an N-terminal chromodomain that binds K36 trimethylated histone H3 (H3K36me3; Fig. S1 *D* and *E*) (19, 20). This prompted us to investigate whether H3K36me3 was required for MRG15-mediated PALB2 chromatin association. In mammalian cells, H3K36me3 is catalyzed by the lysine methyltransferase SET domain containing 2 (SETD2) (21), which facilitates transcription by associating with RNA polymerase II (Pol II) (22, 23) and therefore acts as a general epigenetic mark of active genes (Fig. 1*B*). Strikingly, knockout of SETD2, which is also implicated in HR (24–26), resulted in a concomitant reduction of chromatin-associated PALB2 and H3K36me3 levels (Fig. 1*C* and Fig. S1 *B* and *C*). Similarly, reduced PALB2 chromatin association was found in cells overexpressing lysine demethylase 4A (KDM4A), which counteracts SETD2 (27), or a missense mutant histone

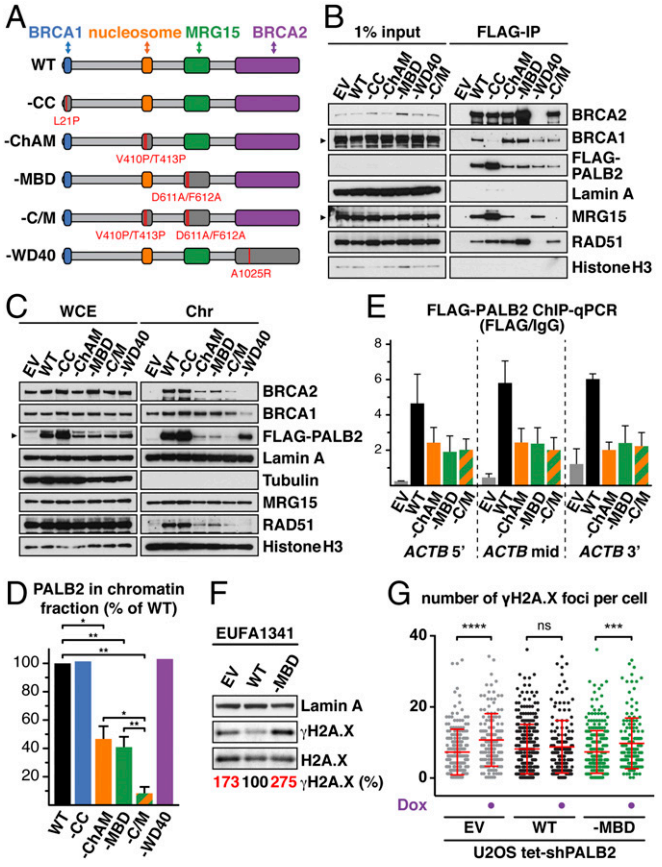

Fig. 2. Ablation of PALB2 binding to MRG15 confers an increased level of DNA stress in unperturbed cells. (*A*) Schematic of PALB2 variants depicting point mutations (red bars) disrupting each domain. (*B*) Anti-FLAG IPs from EUFA1341 cells stably expressing FLAG-PALB2 variants. Lamin A was used as a negative control. (*C*) WB of indicated proteins in the chromatin fraction of EUFA1341 cells stably expressing FLAG-PALB2 variants. (*D*) The levels of PALB2 in the chromatin fraction of cells expressing FLAG-PALB2 variants were quantified and, following normalization against their respective levels in whole-cell extract, expressed as % of WT. Mean values ± SD ($n = 3$). (*E*) ChIP-qPCR quantification of FLAG-PALB2 variants at the *ACTB* gene. (*F*) WB showing the levels of γH2A.X in untreated EUFA1341 cells complemented with FLAG-PALB2 variants. (*G*) The number of γH2A.X foci in U2OS Flp-In T-REx cells stably expressing FLAG-PALB2 variants. Where indicated, cells were treated with 2 μg/mL doxycycline (Dox) for 5 d to induce shRNA targeting endogenous PALB2. Dots represent individual cells and bars mean values ± SD. Statistical significance was determined using two-tailed paired Student's *t* test (*D*) or Mann–Whitney *U* test (*G*). $*P < 0.05$, $**P < 0.01$, $***P < 0.001$, $****P < 0.0001$. EV, empty vector; ns, nonsignificant.

variant H3.3 nonmethylatable at K36 (H3.3 K36M), which is incorporated at transcriptionally active loci independently of replication (28, 29) (Fig. 1*C*). Additionally, our independent genome-wide PALB2 ChIP-sequencing (ChIP-seq) analysis highlighted an enrichment of PALB2 occupancy at H3K36me3-containing genes (Fig. 1 *D* and *E* and Fig. S1 *F* and *G*). ChIP-qPCR quantification of PALB2 occupancy at *ACTB*, *TCOF1*, *WEE1*, and *IRF2BP2*, which were identified as PALB2-bound genes by ChIP-seq analysis both in this study and by Gardini et al. (18), showed a reduced PALB2 level at these loci following inhibition of Pol II-mediated transcription with α-amanitin (α-Am), concomitant with reduced levels of H3K36me3 and chromatin-associated Pol II (Fig. 1*F* and Fig. S2*A*). These observations demonstrate that active transcription is required for PALB2 binding to these genes. Notably, gene set enrichment analysis (GSEA) revealed a higher tendency of PALB2 to bind to periodically expressed genes (Fig. S2*B*), which are associated with a high level of H3K36me3 (30). Conversely, we found little correlation between the level of gene expression and PALB2 association (Fig. S2 *C*–*G*). Together, we conclude that PALB2 associates with active genes, with a preference for periodic genes, via the SETD2/H3K36me3/MRG15 axis. It is plausible that PALB2 has higher affinity for newly marked H3K36me3, which periodically changes during the cell cycle, potentially through a mechanism involving PALB2 chromatin-association motif (ChAM) (14) and/or other PALB2 binding partners.

PALB2 Association with Active Genes Is Necessary to Maintain Genome Integrity. To further examine the physiological role of PALB2 at gene bodies, we first characterized missense mutations blocking PALB2 binding to MRG15. PALB2 MRG15-binding domain (MBD) (31) contains two highly conserved regions: MBD-I (residues 611–629), which includes a MRG-binding FxLP motif (32), and MBD-II (residues 724–737; Fig. S3*A*). Notably, deletion of MBD I or missense mutations within the FxLP motif and other MBD-I conserved residues, such as D611A/F612A (designated as PALB2^{-MBD}), hindered PALB2 binding to MRG15 (Fig. S3 *B* and *C*). PALB2 binding was also blocked by missense mutations of MRG15 at positions 245 and 246 (I245E/L246E), which lie outside the hydrophobic FxLP-binding pocket within the MRG domain (32) (Fig. S1 *D* and *E*). These findings indicate that the PALB2 interaction with MRG15 involves a noncanonical interface.

To consolidate our analysis, we introduced missense mutations ablating other known functional domains of PALB2 (Fig. 2*A*). Through systematic mutagenesis of conserved residues (Fig. S3 *A*, *D*, and *E*), we identified mutations impairing ChAM and generated single (PALB2^{-ChAM}) and double ChAM/MBD (PALB2$^{-C/M}$) mutants. Mutations disrupting PALB2 interaction with BRCA1 (PALB2^{-CC}) and BRCA2 (PALB2^{-WD40}) (7, 33) were also introduced, and each PALB2 variant was stably expressed in PALB2-defective EUFA1341 fibroblasts (5). As expected, BRCA1, MRG15, and BRCA2 were found in protein complexes containing either PALB2^{WT} or PALB2^{-ChAM} but were respectively absent from those containing PALB2^{-CC}, PALB2^{-MBD}, and PALB2^{-WD40} (Fig. 2*B*). Furthermore, cell fractionation analyses established that PALB2^{-CC} and PALB2^{-WD40} associate proficiently with chromatin, whereas PALB2^{-ChAM} and PALB2^{-MBD}, along with BRCA2 and RAD51, showed pronounced reduction of chromatin association, which was further decreased in PALB2$^{-C/M}$ (Fig. 2 *C* and *D*). Importantly, however, our ChIP-qPCR analysis showed comparable levels of PALB2^{-ChAM}, PALB2^{-MBD}, and PALB2$^{-C/M}$ within the *ACTB* gene body (Fig. 2*E*), suggesting that ChAM and MRG15 cooperatively recruit PALB2 to active genes.

While generating EUFA1341 cells complemented with PALB2 variants, we noticed that PALB2^{-MBD} cells grew more slowly than those expressing PALB2^{WT}. Indeed, an increased level of Ser139 phosphorylated histone variant H2A.X (γH2A.X), a marker of DNA stress, was detectable in cells expressing PALB2^{-MBD} compared with PALB2^{WT} (Fig. 2*F*). Similarly, increased levels of γH2AX and γH2AX foci were detectable in U2OS cells stably expressing exogenous PALB2^{-MBD} following the down-regulation of endogenous PALB2 by shRNA (Fig. 2*G* and Fig. S3 *F* and *G*).

To identify the nature of the DNA stress detected in PALB2^{-MBD} cells, we assessed the survival of cells expressing PALB2 variants following treatment with the crosslinking agent mitomycin C (MMC), the TOP1 inhibitor CPT, the DNA polymerase inhibitor aphidicolin (APH), or the ribonucleotide reductase inhibitor hydroxyurea (HU; Fig. 3*A*). Each variant conferred a distinct drug sensitivity signature, with PALB2^{-WD40} most closely matching the phenotype of PALB2-defective cells, exhibiting hypersensitivity to all four drugs. Importantly, cells expressing PALB2^{-MBD} displayed a specific sensitivity to CPT (Fig. 3*A* and Fig. S4 *A* and *B*). Furthermore, compared with cells expressing PALB2^{WT}, a modest but significant impairment of RAD51 foci formation was detectable in PALB2^{-MBD} cells (Fig. 3*B*). In particular, we noticed a marked impairment of RAD51 colocalization with PALB2^{-MBD} in CPT-induced foci (Fig. 3*C*) and a reduced fluorescence intensity of CPT-induced RAD51 foci (Fig. S4*C*). CPT-induced RAD51 foci formation was additionally impaired upon transcription inhibition (Fig. 3*D* and Fig. S4*D*), indicating that RAD51 recruitment is dependent on active transcription.

The impact of CPT treatment on genome stability was further evaluated by examining metaphase chromosome spreads. Strikingly, exposure of PALB2^{-MBD} cells to 10 nM CPT, a dose that typically causes mild replicative stress without inducing substantial DNA breaks (34) (Fig. 4*A*), triggered a significant increase in the number of chromosomal aberrations (Fig. 4 *B* and *C*). In contrast, and as expected, the chromosomal aberration frequency remained unchanged in PALB2^{WT} cells. These results reflect the reduced cellular survival of PALB2^{-MBD} cells upon CPT treatment, further emphasizing the role of MRG15-mediated PALB2 chromatin association in preventing genome instability.

Steady-State Chromatin Association of PALB2 Protects Transcribed Genes from Replication-Associated Stress. At the molecular level, CPT stabilizes the TOP1 cleavage complex, and its toxicity mainly arises from topologically constrained cellular events such as replication or transcription or conflicts between these processes (Fig. 4*D*) (35). Our analysis of chromatin-associated proteins in synchronized HeLa cells revealed no significant enrichment of PALB2, MRG15, or H3K36me3 on S-phase chromatin, contrasting with BRCA1 and RAD51 (Fig. S5*A*). Similarly, PALB2 has not been found to be enriched at stalled replication forks following exposure to HU or CPT in previous studies combining iPOND and proteomics (36, 37). These observations indicate that PALB2 association with chromatin is not induced by general stress associated with DNA replication.

Given the preferential localization of PALB2 to active genes, we hypothesized that MRG15-mediated PALB2 chromatin association has a unique function in the protection of genic regions. Indeed, ChIP-seq analysis of CPT-treated cells identified twice as many γH2A.X peaks in genic regions compared with intergenic regions (Fig. 4*E*), confirming that genic regions are more vulnerable to DNA stress associated with TOP1 defects (38). PALB2^{-MBD} cells exhibited an overall increase in the number of γH2A.X peaks compared with PALB2^{WT} cells, with 398 PALB2-bound genes with γH2A.X peaks detected only in PALB2^{-MBD} cells (Fig. S5*B*, cat. A). The GSEA of these genes revealed a strong enrichment for genes involved in the mitotic spindle and G2/M checkpoint (Fig. S5*C*), which is similar to the top two categories identified in the GSEA for all PALB2-bound genes (Fig. S2*D*). Conversely, the GSEA for PALB2-bound genes with γH2A.X peaks in both PALB2^{-MBD} and PALB2^{WT} cells (Fig. S5*B*, cat. B) or only in PALB2^{WT} cells (Fig. S5*B*, cat. C) showed an enrichment for different categories—namely, damage- and growth factor-responsive genes (Fig. S5 *D* and *E*). These observations support the notion

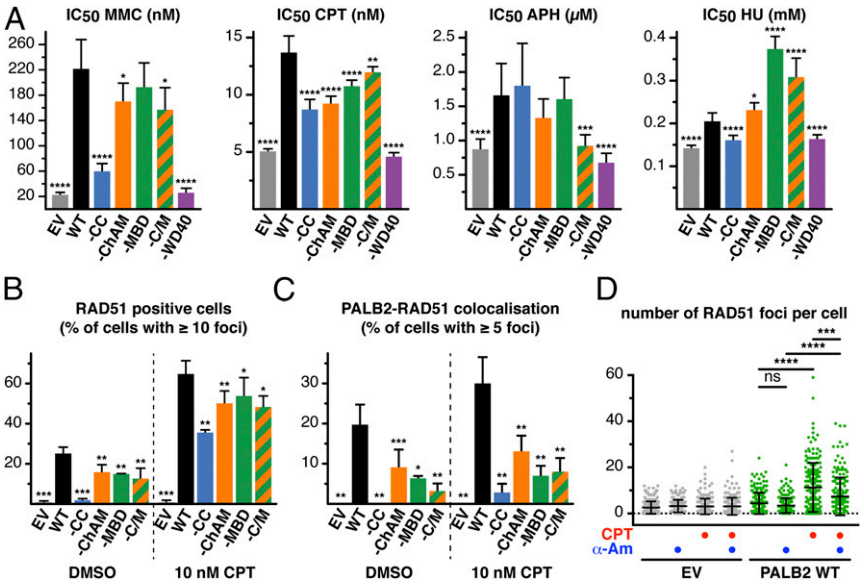

Fig. 3. Ablation of PALB2 binding to MRG15 confers hypersensitivity to CPT. (*A*) The IC_{50} for MMC, CPT, APH, and HU were determined by WST-1 assay. $n = 3$, with two technical replicates. Error bars indicate 95% CI. (*B*) Quantification of RAD51-positive cells (% of cells with ≥10 foci per nucleus). Mean values ± SD ($n \geq 3$, >210 nuclei scored per repeat). (*C*) Quantification of RAD51 and PALB2 colocalization (% of total cells with ≥5 overlapping foci per nucleus). Mean values ± SD ($n \geq 3$, >210 nuclei scored per repeat). (*D*) Quantification of the number of RAD51 foci per cell. Where indicated, cells were treated with CPT or α-Am. Dots represent individual cells and bars mean values ± SD. Statistical significance was determined using the extra sum-of-squares *f* test (*A*), two-tailed paired Student's *t* test (*B* and *C*), or Mann–Whitney *U* test (*D*). $*P < 0.05$, $**P < 0.01$, $***P < 0.001$, $****P < 0.0001$. ns, nonsignificant.

that MRG15-mediated PALB2 chromatin association has a distinctive role in protecting periodic genes.

Additional ChIP-qPCR quantification of γH2A.X at PALB2-bound genes revealed that cells expressing $PALB2^{-MBD}$ triggered H2A.X hyperphosphorylation upon CPT treatment, something that was not seen with PALB2-defective cells (Fig. 4*F* and Fig. S5 *F–I*). This may reflect the partial complementation of EUFA1341 cells by $PALB2^{-MBD}$, mediating a DNA stress response independently of MRG15, such as through BRCA1 interaction. Most importantly, the level of CPT-induced γH2A.X was reduced by DNA replication inhibition with APH, demonstrating that PALB2 in complex with MRG15 suppresses stress arising from DNA replication. In contrast, the level of γH2A.X was intensified by transcription inhibition with α-Am in all cell lines (Fig. S5 *J–M*). Taken together, these observations suggest that, although actively transcribed regions are subject to stress during DNA replication, transcription also helps to protect active genes from DNA stress. It is worth noting, however, that because α-Am is a slow-acting Pol II inhibitor, transcription may have remained active in the early phase of the treatment, resulting in the observed increase of γH2A.X through the conflict of transcription and replication, which was triggered by immediate CPT-induced stress. In this scenario, gradual reduction of PALB2 chromatin association (Fig. 1*F*) and overall inhibition of gene expression might have contributed to an accumulation of DNA stress at active genes.

Lastly, we investigated whether CPT treatment elicits additional PALB2 chromatin association at genic regions. Unexpectedly, our ChIP-qPCR analyses revealed a decrease, rather than an increase, of $PALB2^{WT}$ occupancy at the majority of tested loci in CPT-treated cells (Fig. 5*A* and Fig. S6 *A–C*). In line with this observation, we found an overall reduction of chromatin-associated PALB2 under the same conditions, but no change of H3K36me3 was visible (Fig. S6*D*). Also, a reduced interaction between chromatin-associated PALB2 and MRG15 (Fig. 5 *B* and *C*) and lower MRG15 association with active genes (Fig. S6*E*) were found in CPT-treated cells, indicating that MRG15 plays an important role in controlling the dynamic association of PALB2 with active genes. Interestingly, $PALB2^{-MBD}$ also displayed a consistent reduction in its chromatin association upon CPT treatment (Fig. 5*A* and Fig. S6 *A–C*), suggesting that PALB2 displacement further involves MRG15-independent mechanisms. These observations demonstrate that the dynamic regulation of PALB2 chromatin association is highly complex.

Evidence has emerged in recent years for the importance of histone modifications, which mark chromatin independently of DNA damage, in the regulation of HR. For example, dimethylation of histone H4 at lysine 20 (H4K20me2) contributes to the direct recruitment of HR suppressor 53BP1 (39), whereas non-methylated H4K20 (H4K20me0), which is only found in newly replicated DNA, plays a critical role in the recruitment of TONSL–MMS22L, promoting HR repair in S phase (40). Also, H3K36me3 supports the constitutive association of LEDGF (p75) with active genes, which upon DNA damage recruits the repair factor CtIP to facilitate HR repair (24, 26). Our study establishes that H3K36me3 tethers the MRG15–PALB2 complex to undamaged chromatin, in a manner that makes PALB2 immediately available at active genes and, in this way, protects these more vulnerable regions of the genome from DNA damage (Fig. 5*D*). We propose that, in the event of DNA stress arising from DNA replication, such as that induced by irreversible TOP1-DNA adducts at active genes, PALB2 in complex with BRCA2 and RAD51 is mobilized and, by actively interacting with BRCA1, facilitates the protection and/or repair of nearby replication forks experiencing stress (41, 42). Interestingly, we noticed enhanced levels of BRCA2 and RAD51 association with $PALB2^{-MBD}$ but relatively decreased association of these proteins with $PALB2^{-cc}$ (Fig. 2*B*). These observations could be explained by a model in which full activation of PALB2 through stable interactions with BRCA1, BRCA2, and RAD51 is restricted by its association with MRG15, contributing to the prevention of undesired recombination events in the absence of DNA stress. We envision that PALB2 in complex with MRG15 acts as a local DNA stress sensor, whereas DNA stress swiftly converts it into an effective linker of BRCA1 and BRCA2, providing an elegant mechanism to ensure genome stability. Our study further provides a rationale for the development of small molecules blocking PALB2 binding to MRG15, which may potentiate the effect of CPT-based chemotherapy in the treatment of PALB2-proficient cancers.

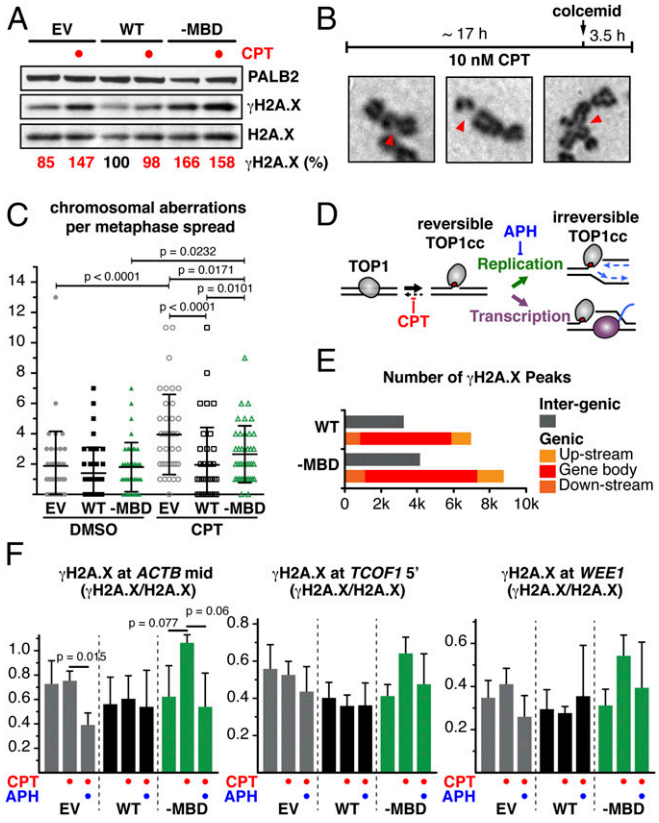

Fig. 4. PALB2 interaction with MRG15 protects active genes during DNA replication. (*A*) WB showing γH2A.X levels in EUFA1341 cells expressing FLAG-PALB2 variants. (*B*) Workflow of metaphase chromosome spread preparation and examples of chromosomal aberrations. (*C*) Aberrant chromosomes per metaphase cell. Dots represent individual cells and bars mean values ± SD (n = 40). P values are for Mann–Whitney U test. (*D*) Diagram depicting the mechanism of TOP1 poisoning by CPT, stabilizing TOP1 cleavage complexes (TOP1cc) at active genes. (*E*) Genome-wide distribution of γH2A.X in EUFA1341 cells expressing PALB2 WT or -MBD mutant, treated with CPT, was determined by ChIP-seq. γH2A.X peaks were categorized as upstream (≤5 kb upstream of gene bodies), downstream (≤5 kb downstream of gene bodies), or intergenic. (*F*) ChIP-qPCR quantification of γH2A.X (γH2A.X/H2A.X ratio). Where indicated, EUFA1341 cells expressing FLAG-PALB2 variants were treated with CPT alone or in combination with APH. Mean values ± SD (n = 3, with triplicate qPCR reactions).

Materials and Methods

Cell Lines and Plasmids. All cell lines were grown at 37 °C in an incubator containing 5% CO_2, using DMEM supplemented with 10% (vol/vol) FBS, penicillin (100 U/mL), and streptomycin (0.1 mg/mL). Plasmids for expression of PALB2, MRG15, and ChAM; HEK293 cells with conditional expression of FLAG-EGFP-PALB2; U2OS cells with constitutive expression of FLAG-PALB2 variants; and EUFA1341 cells complemented with FLAG-PALB2 were generated using standard methods. Oligonucleotides used for site-directed mutagenesis are listed in Table S1. Please refer to *SI Materials and Methods* for detailed procedures.

SiRNA-Mediated Knockdown, Chemical Cell Fractionation, Immunoprecipitation, and Immunofluorescence. ON-TARGETplus SMARTpool siRNAs targeting human BRCA1, MRG15, MRGX, and PALB2 were purchased from Dharmacon and delivered to cells with Dharmafect 1 at a final concentration of 25 nM. The siRNA targeting human SETD2 was previously described (26). Whole-cell extract preparation, chemical cell fractionation, immunoprecipitation, and immunofluorescence analyses were carried out as previously described (14, 43), using antibodies listed in Table S2.

PALB2 Affinity Purification–MS. In brief, HEK293 cells were grown for 1 h in the presence of 2 μg/mL doxycycline to induce FLAG-EGFP-PALB2 expression. Whole-cell lysate was prepared and precleared with IgG agarose beads. FLAG-EGFP-PALB2–containing complexes were captured using GFP-Trap_A (Chromotek) from the precleared whole-cell lysate. Proteins were eluted twice, and elution fractions were pooled before in-solution digestion and quantitative liquid chromatography (LC)–MS/MS analysis. The dataset is available from ProteomeXchange (www.ebi.ac.uk/pride/archive/) with identifier PXD006391. Please refer to *SI Materials and Methods* for detailed procedures.

Cell Survival Assay and IC_{50} Values. In 96-well plates, EUFA1341 cells complemented with FLAG-PALB2 variants were exposed to increasing concentrations of APH (0–20 μM), CPT (0–100 nM), HU (0–2 mM), or MMC (0–2 μM). After 4 d, cell proliferation was measured using WST-1 reagent (Roche Applied Science). Dose–response curves were fitted from the data pool of three independent experiments and the IC_{50} values calculated using Prism 6 (Graphpad Software). Please refer to *SI Materials and Methods* for detailed procedures.

Metaphase Spread Analysis. EUFA1341 cells complemented with FLAG-PALB2 variants were grown to ∼70% confluence and treated with CPT (10 nM) for 17 h. Colcemid (0.1 μg/mL; Millipore) was added to the media and cells harvested after another 3.5 h. Cells were swollen with 0.56% KCl (6 min, room temperature), fixed with methanol/acetic acid (3:1), and dropped onto a microscope slide. Air-dried slides were stained with 0.4% Giemsa (Sigma) and

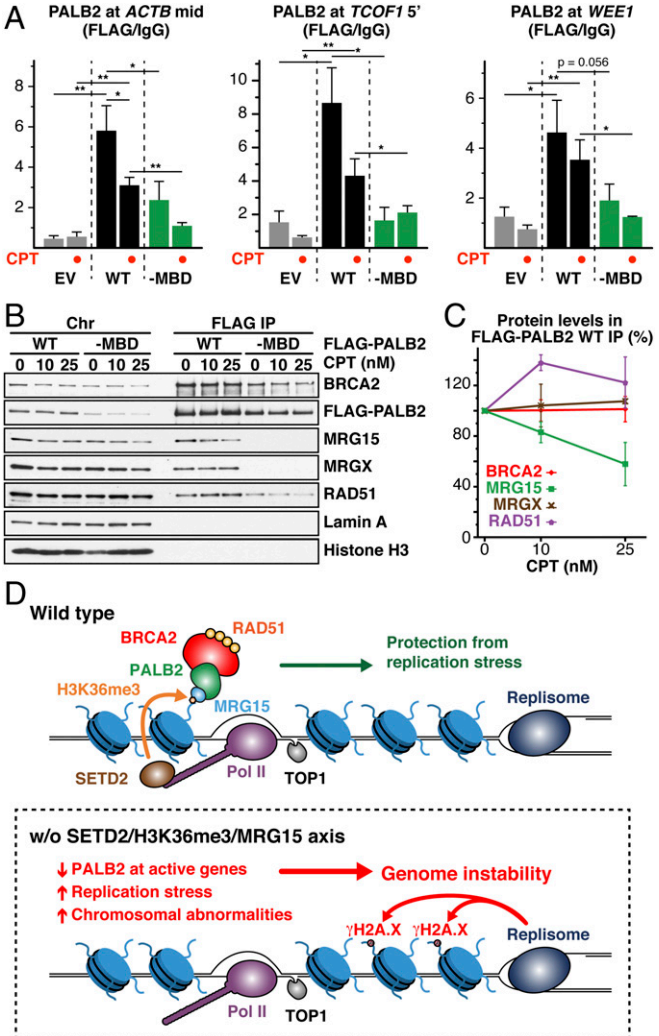

Fig. 5. Chromatin-associated PALB2 is mobilized in response to CPT treatment. (*A*) ChIP-qPCR quantification of FLAG-PALB2 variants. Mean values ± SD (n = 3, with triplicate qPCR reactions). Where indicated, EUFA1341 cells expressing FLAG-PALB2 variants were treated with CPT. Asterisks indicate two-tailed paired Student's t test; $*P < 0.05$, $**P < 0.01$. (*B*) Pull-down experiment showing the interaction between chromatin-associated PALB2 and MRG15 upon CPT treatment. (*C*) Quantification of BRCA2, MRG15, MRGX, and RAD51 levels in FLAG-PALB2 WT IP. Mean values ± SD (n = 2). (*D*) Proposed function of constitutive PALB2 chromatin association.

mounted with Histomount (National Diagnostic). Images were captured with an Olympus BX60 microscope, using *N*-MSI-420–20 camera and Nuance software version 2.10.0 (Cambridge Research & Instrumentation).

ChIP. In brief, EUFA1341 cells complemented with FLAG-PALB2 variants were harvested and fixed with 1% formaldehyde. Nuclei were isolated and genomic DNA was fragmented by partial micrococcal nuclease digestion. The majority of fragments were 150–900 bp in size (1–6 nucleosomes). The digested nuclei were further extracted, lysed by sonication, and cleared by centrifugation. A total of 20 μg of digested chromatin was incubated overnight at 4 °C with 2 μg of antibody. Immunocomplexes were captured with magnetic protein G beads, washed, and ChIP DNA eluted. After cross-link reversal, the samples were extracted twice with Phenol/Chloroform and Ethanol precipitated. The PCR analysis was performed on a Rotorgene Q Real-Time PCR System (Qiagen) using the SensiFAST SYBR No-Rox kit (Bioline). Please refer to *SI Materials and Methods* for full procedures. Where indicated, cells were treated with 10 nM CPT, 0.5 μM APH, or 4 μg/mL α-Am.

ChIP-Seq and GSEA. DNA ChIP fraction was sequenced on the Applied Biosystems SOLiD platforms (SOLiD 5500) and analyzed. The dataset is available from the National Center for Biotechnology Information, Sequence Read Archive (NCBI-SRA) (https://www.ncbi.nlm.nih.gov/Traces/sra/) under accession no. SRP105310. ChIP-seq data of HeLa-S3 H3K36me3 and the corresponding control sample were obtained from ENCODE project (SRA; SRX067462 and SRX067410, respectively). GSEA was performed using the GSEA software provided by the Broad Institute (software.broadinstitute.org/gsea/msigdb/annotate.jsp). Please refer to *SI Materials and Methods* for detailed procedures.

Statistics and Quantitative Analysis. For experiments reproduced at least three times, statistical significance was determined using the indicated test. Data were analyzed using Excel (Microsoft Software) and Prism 6 (Graphpad Software). Quantitative analyses of Western blots (WBs) were performed using the Fiji distribution of ImageJ. For chromatin-bound protein quantitative analyses, the data presented were normalized to the protein level present in the input and expressed as percentage of the control condition.

ACKNOWLEDGMENTS. We thank Dr. H. Joenje (VU University Medical Center, The Netherlands) for sharing the EUFA1341/FA-N fibroblasts; Dr. A. Sartori (Institute of Molecular Cancer Research, Switzerland) for U2OS Flp-In T-REx stable cells; and Prof. C. J. Norbury (Sir William Dunn School of Pathology, United Kingdom) for critical reading of the manuscript. This work was supported by Wellcome Trust Senior Research Fellowship 101009 (to F.E.), Grant-in-Aid for Scientific Research 15K18465 (to R.N.), and Grants-in-Aid for Scientific Research 15H02369, 15K21761, and 15H02369 from MEXT and AMED-CREST (to K.S.). T.C.H. is a recipient of Medical Research Council Grant MC-PC-12001. D.R. is thankful for the support of Singapore Ministry of Education Academic Research Fund Tier 3 Grant MOE2012-T3-1-001 and the NTU Institute of Structural Biology.

1. Erkko H, et al. (2007) A recurrent mutation in PALB2 in Finnish cancer families. *Nature* 446:316–319.
2. Jones S, et al. (2009) Exomic sequencing identifies PALB2 as a pancreatic cancer susceptibility gene. *Science* 324:217.
3. Rahman N, et al.; Breast Cancer Susceptibility Collaboration (UK) (2007) PALB2, which encodes a BRCA2-interacting protein, is a breast cancer susceptibility gene. *Nat Genet* 39:165–167.
4. Reid S, et al. (2007) Biallelic mutations in PALB2 cause Fanconi anemia subtype FA-N and predispose to childhood cancer. *Nat Genet* 39:162–164.
5. Xia B, et al. (2007) Fanconi anemia is associated with a defect in the BRCA2 partner PALB2. *Nat Genet* 39:159–161.
6. Sy SM, Huen MS, Chen J (2009) PALB2 is an integral component of the BRCA complex required for homologous recombination repair. *Proc Natl Acad Sci USA* 106: 7155–7160.
7. Zhang F, Fan Q, Ren K, Andreassen PR (2009) PALB2 functionally connects the breast cancer susceptibility proteins BRCA1 and BRCA2. *Mol Cancer Res* 7:1110–1118.
8. Zhang F, et al. (2009) PALB2 links BRCA1 and BRCA2 in the DNA-damage response. *Curr Biol* 19:524–529.
9. Schlegel BP, Jodelka FM, Nunez R (2006) BRCA1 promotes induction of ssDNA by ionizing radiation. *Cancer Res* 66:5181–5189.
10. Jensen RB, Carreira A, Kowalczykowski SC (2010) Purified human BRCA2 stimulates RAD51-mediated recombination. *Nature* 467:678–683.
11. Liu J, Doty T, Gibson B, Heyer WD (2010) Human BRCA2 protein promotes RAD51 filament formation on RPA-covered single-stranded DNA. *Nat Struct Mol Biol* 17:1260–1262.
12. Thorslund T, et al. (2010) The breast cancer tumor suppressor BRCA2 promotes the specific targeting of RAD51 to single-stranded DNA. *Nat Struct Mol Biol* 17:1263–1265.
13. Benson FE, Stasiak A, West SC (1994) Purification and characterization of the human Rad51 protein, an analogue of E. coli RecA. *EMBO J* 13:5764–5771.
14. Bleuyard JY, Buisson R, Masson JY, Esashi F (2012) ChAM, a novel motif that mediates PALB2 intrinsic chromatin binding and facilitates DNA repair. *EMBO Rep* 13:135–141.
15. Hayakawa T, et al. (2010) MRG15 binds directly to PALB2 and stimulates homology-directed repair of chromosomal breaks. *J Cell Sci* 123:1124–1130.
16. Sy SM, Huen MS, Zhu Y, Chen J (2009) PALB2 regulates recombinational repair through chromatin association and oligomerization. *J Biol Chem* 284:18302–18310.
17. Xia B, et al. (2006) Control of BRCA2 cellular and clinical functions by a nuclear partner, PALB2. *Mol Cell* 22:719–729.
18. Gardini A, Baillat D, Cesaroni M, Shiekhattar R (2014) Genome-wide analysis reveals a role for BRCA1 and PALB2 in transcriptional co-activation. *EMBO J* 33:890–905.
19. Kumar GS, et al. (2012) Sequence requirements for combinatorial recognition of histone H3 by the MRG15 and Pf1 subunits of the Rpd3S/Sin3S corepressor complex. *J Mol Biol* 422:519–531.
20. Zhang P, et al. (2006) Structure of human MRG15 chromo domain and its binding to Lys36-methylated histone H3. *Nucleic Acids Res* 34:6621–6628.
21. Sun XJ, et al. (2005) Identification and characterization of a novel human histone H3 lysine 36-specific methyltransferase. *J Biol Chem* 280:35261–35271.
22. Edmunds JW, Mahadevan LC, Clayton AL (2008) Dynamic histone H3 methylation during gene induction: HYPB/Setd2 mediates all H3K36 trimethylation. *EMBO J* 27:406–420.
23. Yoh SM, Lucas JS, Jones KA (2008) The Iws1:Spt6:CTD complex controls cotranscriptional mRNA biosynthesis and HYPB/Setd2-mediated histone H3K36 methylation. *Genes Dev* 22:3422–3434.
24. Aymard F, et al. (2014) Transcriptionally active chromatin recruits homologous recombination at DNA double-strand breaks. *Nat Struct Mol Biol* 21:366–374.
25. Carvalho S, et al. (2014) SETD2 is required for DNA double-strand break repair and activation of the p53-mediated checkpoint. *eLife* 3:e02482.
26. Pfister SX, et al. (2014) SETD2-dependent histone H3K36 trimethylation is required for homologous recombination repair and genome stability. *Cell Reports* 7:2006–2018.
27. Whetstine JR, et al. (2006) Reversal of histone lysine trimethylation by the JMJD2 family of histone demethylases. *Cell* 125:467–481.
28. Ahmad K, Henikoff S (2002) The histone variant H3.3 marks active chromatin by replication-independent nucleosome assembly. *Mol Cell* 9:1191–1200.
29. Lu C, et al. (2016) Histone H3K36 mutations promote sarcomagenesis through altered histone methylation landscape. *Science* 352:844–849.
30. Dominguez D, et al. (2016) A high-resolution transcriptome map of cell cycle reveals novel connections between periodic genes and cancer. *Cell Res* 26:946–962.
31. Sy SM, Huen MS, Chen J (2009) MRG15 is a novel PALB2-interacting factor involved in homologous recombination. *J Biol Chem* 284:21127–21131.
32. Xie T, Zmyslowski AM, Zhang Y, Radhakrishnan I (2015) Structural basis for multi-specificity of MRG domains. *Structure* 23:1049–1057.
33. Oliver AW, Swift S, Lord CJ, Ashworth A, Pearl LH (2009) Structural basis for recruitment of BRCA2 by PALB2. *EMBO Rep* 10:990–996.
34. Zellweger R, et al. (2015) Rad51-mediated replication fork reversal is a global response to genotoxic treatments in human cells. *J Cell Biol* 208:563–579.
35. Pommier Y (2006) Topoisomerase I inhibitors: Camptothecins and beyond. *Nat Rev Cancer* 6:789–802.
36. Dungrawala H, et al. (2015) The replication checkpoint prevents two types of fork collapse without regulating replisome stability. *Mol Cell* 59:998–1010.
37. Ribeyre C, et al. (2016) Nascent DNA proteomics reveals a chromatin remodeler required for topoisomerase I loading at replication forks. *Cell Reports* 15:300–309.
38. Tuduri S, et al. (2009) Topoisomerase I suppresses genomic instability by preventing interference between replication and transcription. *Nat Cell Biol* 11:1315–1324.
39. Botuyan MV, et al. (2006) Structural basis for the methylation state-specific recognition of histone H4-K20 by 53BP1 and Crb2 in DNA repair. *Cell* 127:1361–1373.
40. Saredi G, et al. (2016) H4K20me0 marks post-replicative chromatin and recruits the TONSL–MMS22L DNA repair complex. *Nature* 534:714–718.
41. Orthwein A, et al. (2015) A mechanism for the suppression of homologous recombination in G1 cells. *Nature* 528:422–426.
42. Schlacher K, Wu H, Jasin M (2012) A distinct replication fork protection pathway connects Fanconi anemia tumor suppressors to RAD51-BRCA1/2. *Cancer Cell* 22: 106–116.
43. Yata K, et al. (2014) BRCA2 coordinates the activities of cell-cycle kinases to promote genome stability. *Cell Reports* 7:1547–1559.
44. Pfister SX, et al. (2015) Inhibiting WEE1 selectively kills histone H3K36me3-deficient cancers by dNTP starvation. *Cancer Cell* 28:557–568.
45. Florens L, et al. (2006) Analyzing chromatin remodeling complexes using shotgun proteomics and normalized spectral abundance factors. *Methods* 40:303–311.
46. Pavelka N, et al. (2008) Statistical similarities between transcriptomics and quantitative shotgun proteomics data. *Mol Cell Proteomics* 7:631–644.
47. Lapytsko A, Kollarovic G, Ivanova L, Studencka M, Schaber J (2015) FoCo: A simple and robust quantification algorithm of nuclear foci. *BMC Bioinformatics* 16:392.
48. Lekomtsev S, Guizetti J, Pozniakovsky A, Gerlich DW, Petronczki M (2010) Evidence that the tumor-suppressor protein BRCA2 does not regulate cytokinesis in human cells. *J Cell Sci* 123:1395–1400.
49. Langmead B, Trapnell C, Pop M, Salzberg SL (2009) Ultrafast and memory-efficient alignment of short DNA sequences to the human genome. *Genome Biol* 10:R25.
50. Nakato R, Itoh T, Shirahige K (2013) DROMPA: Easy-to-handle peak calling and visualization software for the computational analysis and validation of ChIP-seq data. *Genes Cells* 18:589–601.
51. Zhang Y, et al. (2008) Model-based analysis of ChIP-Seq (MACS). *Genome Biol* 9:R137.